The Journal of Chemical Physics

Photodetachment spectroscopy and resonant photoelectron imaging of the 2-naphthoxide anion via dipole-bound excited states

Cite as: J. Chem. Phys. **152**, 214307 (2020); https://doi.org/10.1063/5.0011234
Submitted: 19 April 2020 . Accepted: 18 May 2020 . Published Online: 05 June 2020

Chen-Hui Qian, Guo-Zhu Zhu, Yue-Rou Zhang, and Lai-Sheng Wang

ARTICLES YOU MAY BE INTERESTED IN

Low energy electron impact resonances of anthracene probed by 2D photoelectron imaging of its radical anion
The Journal of Chemical Physics **152**, 174303 (2020); https://doi.org/10.1063/5.0007470

High-resolution photoelectron imaging of MnB_3^-: Probing the bonding between the aromatic B_3 cluster and 3d transition metals
The Journal of Chemical Physics **152**, 244306 (2020); https://doi.org/10.1063/5.0013355

Modern quantum chemistry with [Open]Molcas
The Journal of Chemical Physics **152**, 214117 (2020); https://doi.org/10.1063/5.0004835

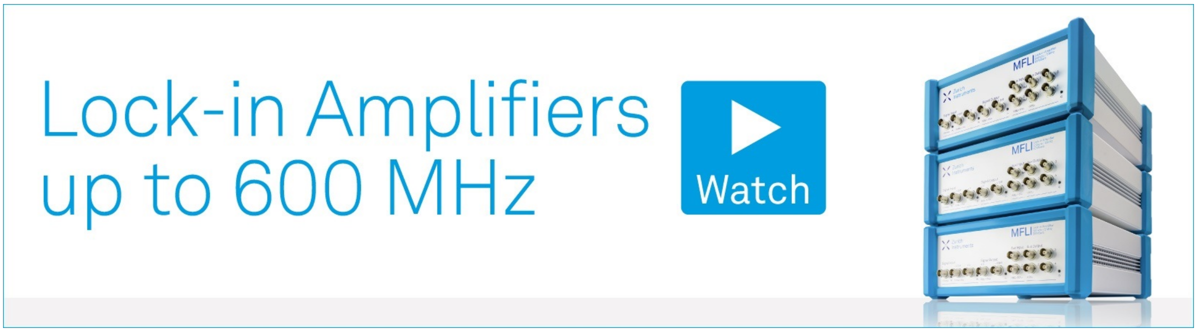

AIP Publishing

The Journal of Chemical Physics

ARTICLE

scitation.org/journal/jcp

Photodetachment spectroscopy and resonant photoelectron imaging of the 2-naphthoxide anion via dipole-bound excited states

Cite as: J. Chem. Phys. **152**, 214307 (2020); doi: 10.1063/5.0011234
Submitted: 19 April 2020 • Accepted: 18 May 2020 •
Published Online: 5 June 2020

Chen-Hui Qian, Guo-Zhu Zhu,[a] Yue-Rou Zhang, and Lai-Sheng Wang[b]

AFFILIATIONS

Department of Chemistry, Brown University, Providence, Rhode Island 02912, USA

[a] **Current address:** Department of Physics and Astronomy, UCLA, Los Angeles, CA 90095, USA.
[b] **Author to whom correspondence should be addressed:** Lai-Sheng_Wang@brown.edu

ABSTRACT

We report a photodetachment spectroscopy and high-resolution resonant photoelectron imaging study of cryogenically cooled 2-naphthoxide anions ($C_{10}H_7O^-$). The photodetachment spectrum revealed a dipole-bound state (DBS) 202(4) cm^{-1} below the detachment threshold and 38 resonances corresponding to the vibrational levels of the DBS. By tuning the detachment laser to these above-threshold resonances, we obtained 38 resonantly enhanced photoelectron spectra, which were highly non–Franck–Condon as a result of mode-selective vibrational autodetachment from the DBS. The resonances were assigned by comparing the resonant and non-resonant photoelectron spectra, assisted by the computed vibrational frequencies. Specifically, vibrational features with low Franck–Condon factors or from Franck–Condon-forbidden vibrational modes were significantly enhanced in the resonant photoelectron spectra, resulting in much richer spectroscopic information. The electron affinity of the 2-naphthoxy radical was measured accurately to be 19 387(4) cm^{-1} or 2.4037(5) eV. In addition, a total of 17 vibrational frequencies were obtained for the 2-naphthoxy radical. In particular, seven Franck–Condon-forbidden out-of-plane bending modes, including the two lowest frequency modes (ν_{48} at 102 cm^{-1} and ν_{47} at 171 cm^{-1}), were observed, demonstrating the advantages of combining photodetachment spectroscopy and resonant photoelectron spectroscopy in obtaining vibrational information for polar radical species via DBS.

I. INTRODUCTION

The 2-naphthol molecule is one of the smallest polycyclic aromatic hydrocarbon (PAH) alcohols, and it has been studied widely in chemistry.[1–3] It is a critical starting material for the syntheses of many important industrial chemicals, such as the Sudan dyes.[4] The 2-naphthol molecule is a model system for photoexcited proton transfers because its acidity can change drastically in the excited states.[5–7] The 2-naphthoxy radical is important in environmental chemistry because it can be produced in the combustion of fossil fuels or oxidation of PAHs.[8,9] The 2-naphthoxy radical and 2-naphthol are also relevant in astrochemistry, and they have been observed to be formed upon ultraviolet photolysis of PAH-ice mixtures, which are present in meteorites and the interstellar medium (ISM).[10,11] Since PAHs are ubiquitous in different astronomical environments,[12] 2-naphthol and the 2-naphthoxy radical could also be present in the ISM. Their ultimate detection in the ISM would require careful laboratory spectroscopic characterization. However, there have been relatively few spectroscopic investigations of the 2-naphthoxy radical.

The ultraviolet-visible absorption spectrum of the 2-naphthoxy radical was first reported in the condensed phase upon photolysis of a 2-naphthol solution.[13] Its infrared and electronic spectra have also been measured in a low-temperature argon matrix,[14] as well as its electron spin resonance spectrum in solution.[15] Anion photoelectron spectroscopy (PES) of 2-naphthoxide has been reported recently by Kregel and Garand (KG) using photoelectron (PE) imaging,[16] where both the ground state and first electronic excited state of the 2-naphthoxy radical were observed. The electron affinity (EA) of 2-naphthoxy was measured to be 2.404(2) eV or 19 390(16) cm^{-1} by KG. In a recent study, photodetachment and photoreactions of the 2-naphthoxide anion were studied by Bieske and co-workers using tandem ion mobility spectrometry, where photodetachment was detected indirectly via the formation of SF_6^-, i.e., using SF_6 as an electron scavenger.[17] In the KG study, five Franck–Condon-active fundamental vibrational modes were observed for the neutral ground state of the 2-naphthoxy radical, as well as two Franck–Condon-forbidden modes observed due to vibronic coupling.[16] The 2-naphthoxy radical possesses a large dipole moment (~4.9 D), which is expected to have a dipole-bound state (DBS) below the detachment threshold of the anion.[18–24] KG observed autodetachment signals attributed to the DBS, and in fact, they took a photodetachment spectrum of 2-naphthoxide in order to avoid the DBS resonances in their PE imaging study. In addition to an electronic excited state of 2-naphthoxide, Bieske and co-workers also observed weak transitions, which were attributed to the DBS in their photodetachment spectrum.[17] A below-threshold peak at 19 180(10) cm^{-1} was suggested to be the likely lowest-lying DBS level.

We have developed a high-resolution PE imaging apparatus in combination with cryogenic cooling of anions from an electrospray ionization (ESI) source.[25] We have observed DBSs as electronically excited states of valence-bound anions below their detachment thresholds for a number of anions with polar molecular cores[26–36] and have been trying to develop resonant PES via DBS.[37–39] Because the dipole-bound electron has very little effect on the neutral core structure, the vibrational frequencies observed in photodetachment spectroscopy via the DBS are the same as the neutral frequencies observed in PES within our experimental uncertainties. It has been demonstrated that photodetachment spectroscopy and resonant-PES via DBS can yield much richer vibrational information for neutral dipolar radicals rivaling infrared spectroscopy.[37–39]

In the current article, we report a combined photodetachment spectroscopy and resonant-PES study of the 2-naphthoxide anion. The EA of the 2-naphthoxy radical is measured more accurately to be 19 387(4) cm^{-1}. A DBS is observed to be 202(4) cm^{-1} below the detachment threshold or 19 185(5) cm^{-1} above the ground state of the 2-naphthoxide anion. Photodetachment spectroscopy was carried out by scanning the laser wavelength across the detachment threshold from 525.60 nm to 480.70 nm, revealing 38 resonances above the threshold, corresponding to the vibrational levels of the DBS. Thirty-eight high-resolution resonant PE images and spectra were obtained by tuning the detachment laser to these DBS resonances. The photodetachment spectrum and the resonant PE spectra are combined to yield a total of 17 fundamental vibrational modes for the 2-naphthoxy radical, including seven Franck–Condon-forbidden out-of-plane bending modes.

II. EXPERIMENTAL METHODS

The experiment was carried out using our third-generation ESI-PES apparatus,[25] equipped with an electrospray ion source,[40] a cryogenically cooled 3D Paul trap,[41] and a high-resolution photoelectron imaging system.[42] The sample was prepared by dissolving 2-naphthol in a MeOH/H_2O (9/1 volume ratio) mixed solvent with a concentration of around 1 mM, followed by adding a small amount of NaOH to increase the pH to ~10 for deprotonation. Anions from the ESI source were directed into the cryogenically cooled ion trap operated at 4.6 K. After being accumulated for 0.1 s and cooled via collision with a He/H_2 (4/1 volume ratio) buffer gas,[41] the cold anions were pulsed out at a 10 Hz repetition rate into a time-of-flight mass spectrometer. The desired 2-naphthoxide anion was selected by using a mass gate and photodetached in the interaction zone of the velocity map imaging (VMI) system by using a tunable nanosecond dye laser. Photoelectrons were focused onto a set of microchannel plates coupled with a phosphor screen. Photoelectron images were captured with a charge-coupled-device camera.

Both the pBasex and Basex programs were used for the data analyses to obtain the inverted images and construct the PE spectra.[43,44] Both programs give similar results, but pBasex yields better inverted images, while Basex is more convenient to construct the PE

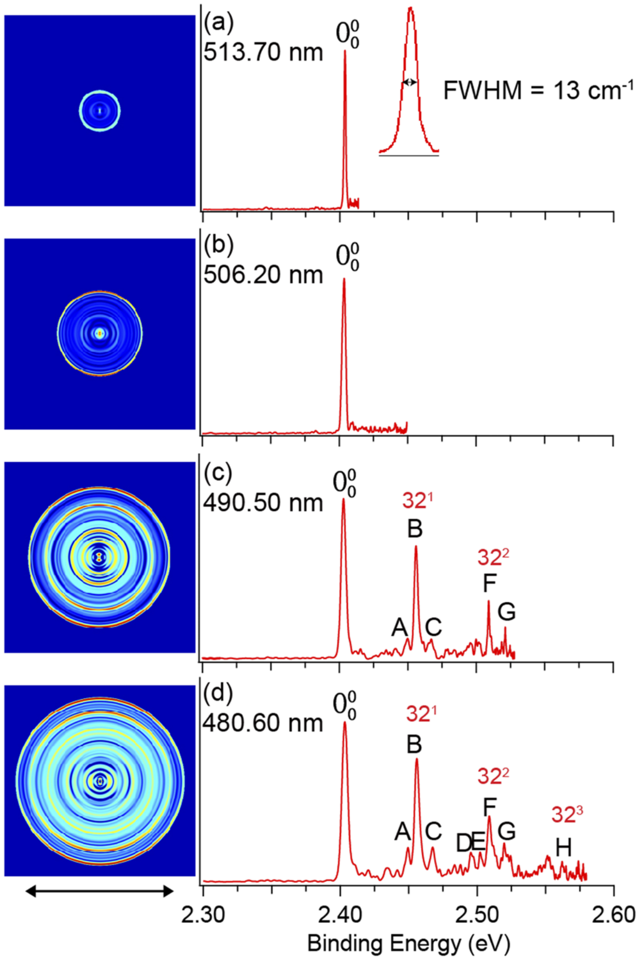

FIG. 1. Non-resonant photoelectron images and spectra of 2-naphthoxide at four detachment wavelengths. The spectra are dominated by one vibrational progression due to the most Franck–Condon-active mode (ν_{32}). The inset of (a) shows the line width of the 0–0 transition near threshold. The double arrow below the image indicates the laser polarization.

spectra. The kinetic energies (KEs) of the photoelectrons were calibrated using the known spectra of Au^- at different photon energies. The kinetic energy resolution was 3.8 cm^{-1} with 55 cm^{-1} KE and was about 1.5% (ΔKE/KE) for KE above 1 eV.[25,42]

The harmonic frequencies and dipole moment of the 2-naphthoxy radical were calculated at the B3LYP/aug-cc-pVTZ level of theory using the Gaussian 09 package.[45]

III. RESULTS

A. Non-resonant photoelectron spectra of 2-naphthoxide

Figure 1 shows the non-resonant PE images and spectra of 2-naphthoxide at four wavelengths. The angular distributions of the images displayed *s*+*d* characters, consistent with the nature of the

TABLE I. Summary of the observed peaks from both the non-resonant and resonant photoelectron spectra of 2-naphthoxide. The binding energies, shifts relative to the 0–0 transition, and assignments are given.

Observed peaks	Binding energy (eV)[a]	Binding energy (cm^{-1})[a]	Shift (cm^{-1})	Assignment	Reference 16 (cm^{-1})	Theo. Frequency (cm^{-1})[b]
0_0^0	2.4034(6)	19 385(5)	0			\
a	2.4160(6)	19 486(5)	102	48^1		103
b	2.4246(6)	19 556(5)	171	47^1		171
c	2.4287(7)	19 589(6)	204	48^2		206
d	2.4345(8)	19 636(6)	251	46^1	248	254
e	2.4408(8)	19 686(6)	302	33^1	303	296
a	2.4497(8)	19 758(6)	373	45^1	368	378
b	2.4562(8)	19 811(6)	426	32^1	422	422
f	2.4585(9)	19 829(7)	444	44^1		449
g	2.4610(8)	19 849(6)	465	31^1		462
h	2.4658(8)	19 888(6)	503	46^2		508
C	2.4670(9)	19 898(7)	513	30^1	512	517
i	2.4712(8)	19 932(6)	554	$33^1 46^1$		550
j	2.4771(7)	19 979(6)	594	$32^1 47^1$		593
k	2.4790(9)	19 994(7)	610	29^1		616
l	2.4835(8)	20 031(6)	646	42^1		656
m	2.4865(9)	20 055(7)	670	$32^1 46^1$		676
n	2.4885(12)	20 071(9)	686	$44^1 46^1$		703
o	2.4922(10)	20 101(8)	716	28^1	721	712
D	2.4954(7)	20 127(6)	742	27^1	743	748
p	2.5010(8)	20 172(6)	787	$29^1 47^1$		782
E	2.5024(6)	20 183(5)	798	$32^1 45^1$		800
q	2.5053(10)	20 207(8)	822	$30^1 33^1$		813
F	2.5090(9)	20 236(7)	852	32^2	846	844
r	2.5110(8)	20 253(6)	869	$32^1 44^1$		871
s	2.5128(7)	20 267(6)	882	$44^2/31^1 32^1$		898/884
t	2.5144(8)	20 280(6)	895	$42^1 46^1/30^1 45^1$		901/895
u	2.5169(8)	20 300(6)	915	$29^1 33^1$		907
v	2.5184(9)	20 312(7)	928	$27^1 47^1/32^1 46^2$		919/930
G	2.5208(9)	20 332(7)	947	$30^1 32^1$	943	939
w	2.5243(7)	20 360(5)	975	$36'^1$		954
x	2.5265(9)	20 378(7)	993	$27^1 46^1$		1002
y	2.5363(6)	20 457(5)	1072	$32^1 42^1$		1069
z	2.5393(9)	20 481(7)	1096	$32^2 46^1$		1098
α	2.5416(9)	20 499(7)	1115	$27^1 45^1$		1134
β	2.5453(11)	20 529(9)	1145	$21^1/28^1 32^1/29^1 30^1$		1142/1134/1128
H	2.5629(8)	20 671(6)	1286	32^3		1266

[a] The uncertainty of the measurement is given in the parentheses.

[b] Theoretical frequencies are from Table S1.

highest occupied molecular orbital of 2-naphthoxide, which is a delocalized π orbital.[16] The two spectra at the higher photon energies in Figs. 1(c) and 1(d) are similar to those reported by KG recently. We also took two spectra closer to the detachment threshold to obtain a more accurate electron affinity (EA) for the 2-naphthoxy radical. The near-threshold spectrum in Fig. 1(a) gives the highest resolution measurement for the 0–0 transition, with a full width at half maximum (FWHM) of 13 cm^{-1} mainly due to rotational broadening.[26,37] This spectrum yielded an EA of 2.4033(6) eV, compared with 2.404(2) eV reported recently by KG.[16] The uncertainty was obtained from the peak width [see the inset of Fig. 1(a)]. We will show below that our photodetachment spectrum yields an even more accurate EA value. The PE spectra of 2-naphthoxide are dominated by one major vibrational progression (ν_{32}), represented by peaks B, F, and H. This most Franck–Condon-active mode involves the ring stretching motion with a measured frequency of 426 cm^{-1} compared to 422 cm^{-1} reported by KG.[16] We also did a Franck–Condon simulation, as compared with the experimental data in Fig. S1, where the PE spectrum is compared with the photodetachment spectrum to be discussed below. The electron binding energies (BE), the energy shifts relative to the 0–0 transition, and the assignment of the PES features are given in Table I, together with the much richer vibrational features observed in the resonant photoelectron spectra to be discussed below.

B. Photodetachment spectroscopy

The photodetachment spectrum was obtained by scanning the detachment laser wavelength across the detachment threshold from 525.60 nm to 480.70 nm and monitoring the total electron yield. A scan step of 0.1 nm was used to take the photodetachment spectrum shown in Fig. 2, followed by finer scans for each observed peak with 0.01 nm/step to determine the peak positions more accurately. The arrow indicates the position of the EA at 19 385 cm^{-1} measured from the non-resonant PE spectrum from Fig. 1(a). Because of the *s*+*d* character of the outgoing electron, there is a prompt rise of detachment cross section at the threshold following the Wigner threshold law.[46] On the basis of the rising edge, we were able to obtain a slightly more accurate EA for 2-naphthoxy at 19 387(4) cm^{-1} than that from the PE spectra discussed above. The EA was evaluated by taking the mid-point of the rising edge, and the uncertainty was estimated from several measurements and by considering the step size of the scan. We calculated the dipole moment of the 2-naphthoxy radical to be 4.9 D at the B3LYP/aug-cc-pVTZ level of theory, which is significantly larger than the critical 2.5 D dipole moment for supporting a DBS,[18] as already observed.[16,17] We observed a weak peak below threshold (labeled 0 in Fig. 2), which should correspond to the ground vibrational level of the expected DBS observed due to resonant two-photon detachment (R2PD). The inset of Fig. 2 shows the R2PD PE image, where the weak outer ring with high photoelectron kinetic energy came from detachment from the DBS ground vibrational level by the second photon within the same laser pulse (~6 ns).

The position of peak 0 is measured to be 19 185(5) cm^{-1} (521.25 nm) above the ground state of 2-naphthoxide, in agreement with the recent report by Bieske and co-workers,[17] who observed a weak below-threshold peak at 19 180(10) cm^{-1} in their photodetachment spectrum and attributed it to be the likely lowest-lying DBS level. The energy separation of 202(4) cm^{-1} between peak 0 and the detachment threshold represents the DBS binding energy of 2-naphthoxide. This binding energy of 202 cm^{-1} is significantly larger than the 97 cm^{-1} DBS binding energy observed in phenoxide.[26] The dipole moment of 2-naphthoxy (4.9 D) is only slightly higher than that of phenoxy (4.0 D), indicating that the larger polarizability of the naphthyl group compared to the phenyl ring contributes substantially to the electron binding in the DBS.

Above threshold, the photodetachment spectrum reveals a high density of resonances on top of the detachment continuum. A total of 38 peaks (labeled from 1 to 38) were observed in a spectral range of about 1400 cm^{-1}. These peaks, aka vibrational Feshbach resonances, correspond to vibrational levels of the DBS and were observed via vibrational autodetachment through vibronic coupling. The peak positions, shifts relative to the ground vibrational state of the DBS, and their assignments are given in Table II. The assignments of the peaks are done from the resonant photoelectron spectra (*vide infra*), as well as by comparison with calculated vibrational frequencies for the 2-naphthoxy radical.

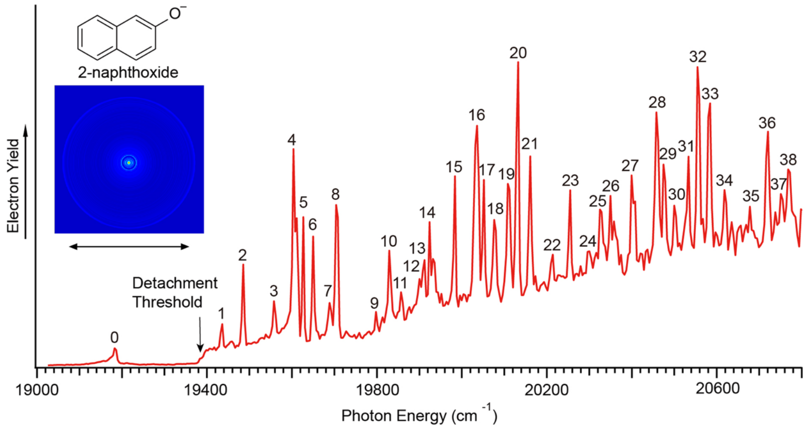

FIG. 2. Photodetachment spectrum of 2-naphthoxide. The down arrow shows the detachment threshold, which is measured slightly more accurately as 19 387(4) cm^{-1} than that from the PE spectrum in Fig. 1(a). Peak 0 below the detachment threshold represents the ground vibrational level of the DBS. The inset shows the resonant two-photon PE image taken at the wavelength of peak 0 (521.25 nm). The double arrow below the image shows the direction of the laser polarization. Thirty-eight above-threshold peaks are observed corresponding to vibrational levels of the DBS.

TABLE II. Summary of the resonances observed in the photodetachment spectrum of 2-naphthoxide in Fig. 2. The corresponding wavelengths, photon energies, energy shifts with respect to peak 0, and assignments are given.

Observed peaks	Wavelength (nm)	Photon energy (cm^{-1})[a]	Shift (cm^{-1})	Assignment	Theo. frequencies (cm^{-1})[b]
0	521.25	19 185(5)	0	Ground state DBS	
1	514.58	19 433(5)	248	$46'^{1}$	254
2	513.20	19 486(5)	301	$33'^{1}$	296
3	511.28	19 559(5)	374	$45'^{1}/47'^{1}48'^{2}$	378/377
4	509.87	19 613(5)	428	$32'^{1}$	422
5	509.55	19 625(5)	440	$44'^{1}$	449
6	508.92	19 649(5)	464	$31'^{1}$	462
7	507.95	19 687(5)	502	$46'^{2}$	508
8	507.47	19 706(5)	521	$30'^{1}$	517
9	505.10	19 798(5)	613	$29'^{1}/44'^{1}47'^{1}$	611/620
10	504.33	19 828(5)	643	$42'^{1}$	647
11	503.62	19 856(5)	671	$32'^{1}46'^{1}$	676
12	502.48	19 901(5)	716	$28'^{1}$	712
13	502.24	19 911(5)	726	$32'^{1}33'^{1}$	718
14	501.95	19 922(5)	737	$27'^{1}$	748
15	500.48	19 981(5)	796	$32'^{1}45'^{1}$	800
16	499.07	20 037(5)	852	$32'^{2}$	844
17	498.68	20 053(5)	868	$32'^{1}44'^{1}$	871
18	498.10	20 076(5)	891	$44'^{2}/31'^{1}32'^{1}/42'^{1}46'^{1}$	898/884/901
19	497.28	20 109(5)	924	$32'^{1}46'^{2}/27'^{1}47'^{1}$	930/919
20	496.77	20 130(5)	945	$30'^{1}32'^{1}$	936
21	496.03	20 160(5)	975	$36'^{1}$	954
22	494.77	20 211(5)	1026	$24'^{1}$	1018
23	493.69	20 256(5)	1071	$32'^{1}42'^{1}$	1069
24	492.65	20 298(5)	1113	$32'^{1}44'^{1}46'^{1}/27'^{1}45'^{1}$	1125/1126
25	491.93	20 328(5)	1143	$28'^{1}32'^{1}/30'^{1}42'^{1}$	1140/1164
26	491.40	20 350(5)	1165	$27'^{1}32'^{1}$	1170
27	490.05	20 406(5)	1221	$32'^{2}45'^{1}$	1222
28	488.79	20 459(5)	1274	$32'^{3}$	1266
29	488.43	20 474(5)	1289	$32'^{2}44'^{1}$	1293
30	487.72	20 504(5)	1319	$32'^{1}42'^{1}46'^{1}$	1323
31	487.00	20 534(5)	1349	$27'^{1}32'^{1}47'^{1}$	1341
32	486.50	20 555(5)	1370	$30'^{1}32'^{2}$	1361
33	485.81	20 584(5)	1399	$32'^{1}36'^{1}$	1376
34	484.95	20 621(5)	1436	$29'^{1}30'^{1}33'^{1}/21'^{1}33'^{1}/28'^{2}/27'^{1}44'^{1}46'^{1}$	1424/1438/1424/1451
35	483.55	20 680(5)	1495	$32'^{2}42'^{1}$	1491
36	482.65	20 719(5)	1534	$27'^{1}29'^{1}47'^{1}/32'^{3}46'^{1}/27'^{1}32'^{1}45'^{1}$	1530/1520/1548
37	481.85	20 753(5)	1568	$21'^{1}32'^{1}/28'^{1}32'^{2}$	1564/1556
38	481.46	20 770(5)	1585	$9'^{1}$	1580

[a] Uncertainty is given by the number in the parentheses.

[b] Theoretical frequencies are from Table S1.

The dipole-bound electron is in a highly diffuse orbital and has a negligible effect on the structure of the neutral core. To further illustrate the similarity of the neutral core of the DBS and the neutral radical, we compared the photodetachment spectrum and the PE spectrum in Fig. S1, where we overlap the photodetachment spectrum and the PE spectrum at 480.60 nm by aligning their corresponding 0–0 transitions. Furthermore, a Franck–Condon simulation is also presented in the figure, which was calculated using the B3LYP/Aug-cc-pVTZ level of theory, while the vibrational frequencies were scaled by a factor of 0.975 to better fit the experimental

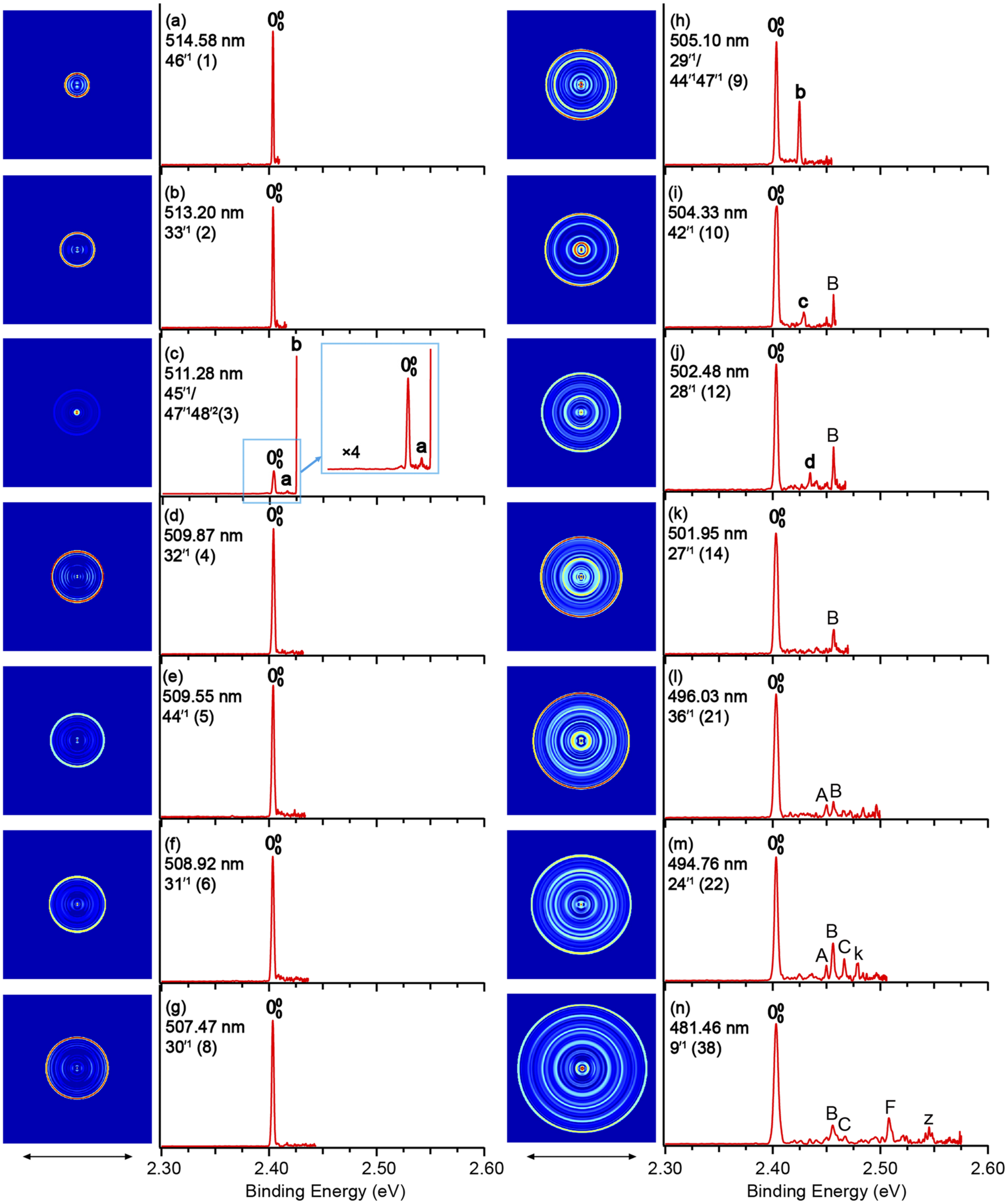

FIG. 3. Resonant PE images and spectra of 2-naphthoxide taken at wavelengths corresponding to excitations to fundamental vibrational levels of the DBS. The wavelength and the assignments of the DBS levels are also given. The number in the parentheses following the vibrational assignments corresponds to the peak label in Fig. 2. The enhanced peaks, i.e., the 0–0 transition, due to the vibrational autodetachment are labeled in **bold** face. The double arrows below the images indicate the direction of the laser polarization.

results. It is shown that there is a good match between the major Franck–Condon-active vibrational features in the two spectra, providing direct evidence that the vibrational frequencies of the DBS observed in the photodetachment spectrum are equivalent to those of the neutral radical within our experimental accuracy. It is important to point out that there are many more non–Franck–Condon vibrational transitions observed in the photodetachment spectrum due to the resonant excitation from the anion ground state to the DBS levels and vibronic coupling. It is these non–Franck–Condon excitations in the photodetachment spectrum that yielded richer and more accurate vibrational information for the 2-naphthoxy radical via resonant PES.

C. Resonant photoelectron spectra of 2-naphthoxide

The resonant PE spectra were taken by tuning the detachment laser wavelength to the positions of the above-threshold DBS resonances observed in the detachment spectrum. The 38 resonant PE spectra are presented in Fig. 3 (14), Fig. 4 (8), Fig. 5 (2), and Fig. S2 (14). Comparing these resonant PE spectra to those in Fig. 1, we can readily see that one or more vibrational peaks are enhanced in the resonant spectra (labeled in **bold face**), as well as a plethora of additional peaks (*a-z*, *α-β*) that are not observed in the non-resonant PE spectra, either because of their low Franck–Condon factors or because they are Franck–Condon-forbidden. Figure 3 displays resonant PE spectra corresponding to excitations to fundamental vibrational levels of the DBS, whereas Fig. 4 shows resonant PE spectra following excitation to combinational DBS levels involving two vibrational modes. At higher photon energies, the density of vibrational levels increases significantly. Hence, there can be overlapping vibrational levels that can be excited simultaneously, producing relatively complicated resonant PE spectra, as shown in Fig. 5. Figure S2 documents the remaining 14 resonant PE spectra, which are not discussed in detail in the main text. All the observed peaks, their binding energies, energy shifts relative to the 0–0 transition, and their assignments are given in Table I.

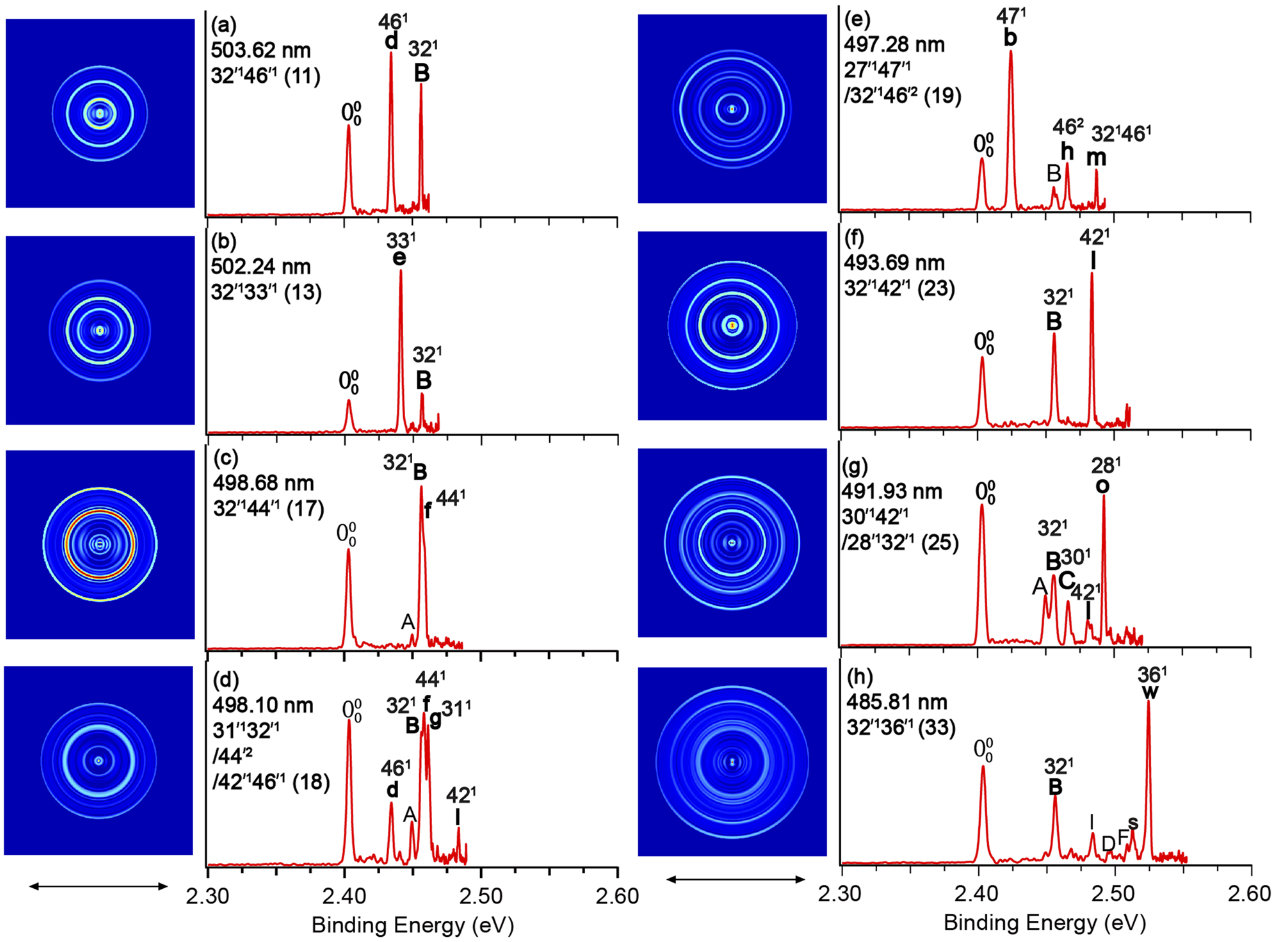

FIG. 4. Resonant PE images and spectra of 2-naphthoxide taken at wavelengths corresponding to excitations to DBS levels consisting of two vibrational modes. The wavelengths and the assignments are also given. The number in the parentheses following the vibrational assignment corresponds to the peak label in Fig. 2. The enhanced vibrational peaks are labeled in **bold** face. The double arrows below the images indicate the direction of the laser polarization.

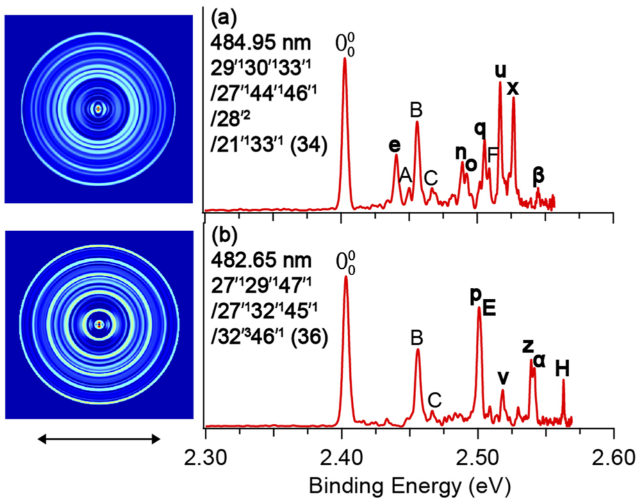

FIG. 5. Two resonant PE images and spectra of 2-naphthoxide taken at higher photon energies corresponding to peak 34 (a) and peak 36 in Fig. 2. These complicated spectra are due to excitations to overlapping vibrational levels of the DBS, producing multiple enhanced peaks (labeled in **bold** face). The double arrows below the images indicate the direction of the laser polarization.

IV. DISCUSSION

Two processes contribute to the resonant PE spectra: (1) the non-resonant detachment process corresponding to the rising continuum in the photodetachment spectrum in Fig. 2 and (2) the resonantly enhanced vibrational autodetachment from the DBS levels. The non-resonant photodetachment obeys the Franck–Condon principle, while the resonant PE spectra are highly non–Franck–Condon. As shown previously,[26–39] autodetachment from vibrational levels of the DBS follows the $\Delta v = -1$ propensity rule under the harmonic approximation,[47,48] which means that only one vibrational quantum can be coupled to the dipole-bound electron to induce autodetachment. The $\Delta v = -1$ propensity rule is a direct manifestation of the similarity between the structures of the DBS and the neutral and was first derived for autoionization from Rydberg states of H_2.[47] For example, if a resonant excitation occurs to the DBS vibrational level $\nu_x{'}^n$ (the *n*th quantum of the $\nu_x{'}$ mode; the prime $'$ refers to DBS modes), autodetachment will lead to the $(n - 1)$th level of the same vibrational mode in the neutral ($\nu_x{}^{n-1}$), which will be enhanced in the resonant PE spectrum. For autodetachment from a combinational vibrational level ($\nu_x{'}^n \nu_y{'}^m \ldots$) of the DBS, the final neutral state could be either $\nu_x{'}^{n-1} \nu_y{'}^m \ldots$ or $\nu_x{'}^n \nu_y{'}^{m-1} \ldots$, producing multiple enhanced vibrational peaks in the resonant PE spectra, provided that the vibrational frequencies of $\nu_x{'}$ or $\nu_y{'}$ are higher than the DBS binding energy. In the current case, only modes ν_{48} and ν_{47} have calculated frequencies less than the DBS binding energy of 204 cm^{-1} (Table S1).

A. Resonant PE spectra: Excitations of the fundamental vibrational levels of the DBS

Figure 3 shows the resonant PE spectra, which resulted from excitations to fundamental vibrational levels of the DBS, leading to enhancement of the 0-0 transition according to the $\Delta v = -1$ propensity rule. In Figs. 3(a), 3(b), and 3(d)–3(g), only the 0–0 transition was observed upon tuning the detachment laser to peaks 1, 2, 4–6, and 8, respectively, in Fig. 2. They can be assigned to excitations to $46'^1$, $33'^1$, $32'^1$, $44'^1$, $31'^1$, and $30'^1$ of the DBS, respectively, without ambiguity. The measured vibrational frequencies in the photodetachment spectrum are in good agreement with the computed frequencies (Table II). The $32'^1$ transition (peak 4) is the most intense peak in the low binding energy part of the photodetachment spectrum (Fig. 2), consistent with the fact that the ν_{32} mode is the most Franck–Condon-active mode in the non-resonant PE spectra (Fig. 1 and Fig. S1). The vibrational frequency for the $\nu_{32}{'}$ mode of the DBS measured from the photodetachment spectrum is 428 cm^{-1} (Table II), which is identical to the frequency of the ν_{32} mode (426 cm^{-1}, Table I) measured from the non-resonant PE spectrum for the neutral 2-naphthoxy radical within our experimental uncertainties. The current ν_{32} frequency agrees with that reported by KG (422 cm^{-1}).[16]

In Figs. 3(i)–3(n), the enhancement of the 0-0 transition could be observed more directly by comparing with the non-resonant PE spectra in Fig. 1 because one or more Franck–Condon-active modes appeared in the resonant PE spectra. For example, the relative intensity of the 0-0 transition in all these spectra is significantly higher than peak B (32^1), compared to that in Fig. 1. This observation suggests that all these resonant PE spectra correspond to excitation to a fundamental vibrational level of the DBS, following a $\Delta v = -1$ autodetachment. The assignments of the DBS levels are given in Fig. 3, and the measured frequencies for the corresponding vibrational modes are in good agreement with the calculated frequencies (Table II). Among the six modes, only mode ν_{27} has any Franck–Condon activity in the non-resonant PE spectra, yielding a frequency of 742 cm^{-1} (Table I), which is compared with the frequency in the DBS at 737 cm^{-1} (Table II). Two new and weak features were observed in Fig. 3(i) (peak *c*) and Fig. 3(j) (peak *d*), which are assigned to 48^2 and 46^1 (Table I), respectively, according to their binding energies. However, these new peaks do not correspond to excitations to any combinational vibrational levels of the DBS involving these modes. Similar weak features have been observed previously and were attributed to intramolecular inelastic rescattering,[31] where the autodetached outgoing electron excites low-frequency modes of the neutral core.

Figure 3(h) shows a very strong new peak *b*. Its binding energy indicates that it corresponds to mode ν_{47} (Table I), but it is unlikely due to the inelastic rescattering mechanism mentioned above, which usually yields very weak features. It turns out that the combinational vibrational level $44'^1 47'^1$ is nearly degenerate with $29'^1$ (Table II), and both could be excited simultaneously. The excitation of $29'^1$ yielded the enhanced 0-0 transition, whereas that of $44'^1 47'^1$ gave rise to the new peak *b* via coupling of one quantum of $44'^1$ to the dipole-bound electron. Overlapping vibrational levels become more common at higher excitation energies, as will be discussed below.

Figure 3(c) corresponds to excitation to the $45'^1$ DBS level with a measured vibrational frequency of 374 cm^{-1} for the $\nu_{45}{'}$ mode (Table II). The ν_{45} mode is also observed in the non-resonant PE spectrum (Table I) due to vibronic coupling[16] because it is an out-of-plane mode and is symmetry-forbidden. Two more features in Fig. 3(c) are surprising. One is the near-threshold strong cutoff (peak *b*), corresponding to mode ν_{47} with a vibrational frequency of

171 cm^{-1}, as observed in Fig. 3(h) (Table I). The second surprising feature in Fig. 3(c) is the observation of a weak peak *a*, which corresponds to mode ν_{48}, the lowest frequency mode of 2-naphthoxy (103 cm^{-1}, Table S1). Peak *a* yields an experimental frequency of 102 cm^{-1} for this bending mode (Table I), in excellent agreement with the computed value. These extra features suggest the excitation of a combinational level of $47'^{1}48'^{2}$, which is nearly degenerate with $45'^{1}$. Coupling of two quanta of ν_{48}' ($48'^{2}$) with the dipole-bound electron would yield peak *b*, whereas coupling of $47'^{1}48'^{1}$ with the DBS electron would give rise to peak *a*. Note that one quantum of neither ν_{47} nor ν_{48} is sufficient to induce autodetachment. These $\Delta v = -2$ autodetachment processes can happen due to anharmonicity[47] and have been observed previously, usually for low-frequency bending modes, which tend to have large anharmonicity.[28–34,37–39]

B. Resonant PE spectra: Excitations to combinational vibrational levels ($\nu_x'^{1}\nu_y'^{1}$) of the DBS

For excitations to combinational vibrational levels ($\nu_x'^{1}\nu_y'^{1}$) of the DBS, either vibrational quantum can couple to the dipole-bound electron to induce autodetachment (except ν_{47} and ν_{48} in the current case), resulting in the enhancement of either the ν_x^{1} or ν_y^{1} final vibrational state in the resonant PE spectra. In particular, if the ν_x and ν_y modes are not Franck–Condon active, they can be "lit up" in the resonant PE spectra, greatly expanding the spectroscopic content of PES. Figure 4 displays eight resonant PE spectra, all involving excitation to a combinational level of two modes. Since the ν_{32} mode is the most Franck–Condon-active (Fig. 1), a majority of the combinational levels involve this mode ($32'^{1}\nu_y'^{1}$), resulting in the enhancement of the ν_y^{1} vibrational level in the resonant PE spectra. Figure S2 presents more resonant PE spectra involving excitations to combinational levels, some of which are quite complicated involving three modes or overtones.

Figures 4(a)–4(c), 4(f), and 4(h) are due to excitation to combinational levels $32'^{1}46'^{1}$, $32'^{1}33'^{1}$, $32'^{1}44'^{1}$, $32'^{1}42'^{1}$, and $32'^{1}36'^{1}$, respectively. The 46^{1} (peak *d*), 33^{1} (peak *e*), 44^{1} (peak *f*), 42^{1} (peak *l*), and 36^{1} (peak *w*) transitions appeared prominently in the resulting resonant PE spectra. Only 46^{1} and 33^{1} were observed in the non-resonant PE spectra as weak features (Fig. 1); the appearance of the ν_{46} bending mode was due to vibronic coupling.[16] Figures 4(d), 4(e), and 4(g) display enhancement of multiple peaks, which were not observed in the non-resonant PE spectra, as a result of excitation to overlapping vibrational levels of the DBS, as already discussed in a couple of cases in Fig. 3. For example, the spectrum in Fig. 4(d) was taken at the wavelength of peak 18 in Fig. 2, corresponding to an excitation energy of 891 cm^{-1} above the ground vibrational level of the DBS (Table II). Three vibrational levels with different combinational modes have almost the same excitation energies, $31'^{1}32'^{1}$ (892 cm^{-1}), $44'^{2}$ (888 cm^{-1}), and $42'^{1}46'^{1}$ (891 cm^{-1}). These nearly degenerate levels were excited simultaneously, resulting in the complicated resonant PE spectrum in Fig. 4(d) with five enhanced final vibrational levels: 46^{1}, 32^{1}, 44^{1}, 31^{1}, and 42^{1}. Similarly, in Fig. 4(e), the final vibrational states 47^{1} (peak *b*), 46^{2} (peak *h*), and $32^{1}46^{1}$ (peak *m*) are shown to be enhanced due to excitation of the nearly degenerate $27'^{1}47'^{1}$ and $32'^{1}46'^{2}$ vibrational levels of the DBS. Since the frequency of ν_{47}' is less than the DBS binding energy as mentioned above, only the enhanced 47^{1} final vibrational level is observed as a result of excitation to the $27'^{1}47'^{1}$ DBS level. The resonant PE spectrum in Fig. 4(g) can be understood similarly as a result of excitation of the overlapping DBS vibrational levels of $30'^{1}42'^{1}$ and $28'^{1}32'^{1}$.

The resonant PE spectra shown in Fig. 4 revealed six final vibrational states of the 2-naphthoxy radical, 47^{1}, 44^{1}, 42^{1}, 36^{1}, 31^{1}, 28^{1}, which were not observed in the non-resonant PE spectra. Some of these final states also appeared in other resonant PE spectra shown in Fig. S2. Several of these vibrational modes also appeared in the photodetachment spectrum (Fig. 2). The measured vibrational frequencies of these modes from the resonant PE spectra are given in Table I, in comparison with the calculated frequencies. The assignments of the corresponding DBS levels are given in Table II.

C. Resonant PE spectra: Excitations to multiple overlapping DBS vibrational levels

As the excitation energy increases, the vibrational density of states in the DBS increases dramatically. Thus, level congestion or accidental degeneracy of vibrational levels occurs more frequently because of the different possible combinational levels. Fortunately, not all levels have sufficient excitation cross sections to be observed. Those that have been observed tended to involve combinational levels of Franck–Condon-active modes. We have already seen accidental vibrational level degeneracy in Figs. 3 and 4. More are shown in Fig. S2. Figure 5 displays the two most complicated resonant PE spectra observed in this study, each involving multiple nearly degenerate combinational vibrational levels of the DBS. The assignments of these DBS vibrational levels can be tricky, but they can be done with reasonable confidence using the enhanced vibrational peaks in the resonant PE spectra by applying the $\Delta v = -1$ propensity rule and the observed vibrational frequencies in other spectra or the computed vibrational frequencies as a guide.

Figure 5(a) exhibits seven new or enhanced peaks labeled *e*, *n*, *o*, *q*, *u*, *x*, and *β* with the following energy shifts relative to the 0–0 transition: 302 cm^{-1}, 686 cm^{-1}, 716 cm^{-1}, 822 cm^{-1}, 915 cm^{-1}, 993 cm^{-1}, and 1145 cm^{-1}, as shown in Table I. These rich vibrational final states must imply excitation to overlapping DBS vibrational levels of different combinational modes. The resonant PE spectrum was taken at 484.95 nm (peak 34 in Fig. 2), which is 1436 cm^{-1} above the DBS ground state (Table II). Hints about which combinational modes were excited could be glimpsed from the enhanced vibrational peaks in Fig. 5(a). Due to the obvious enhancement of the vibrational peak 33^{1} (peak *e*), the other component for the combinational DBS level should be 1134 cm^{-1} (1436–302 cm^{-1}), which could be assigned to peak *β* within our experimental accuracy. The calculated frequency for the ν_{21} mode is 1142 cm^{-1} (Table S1). Hence, the DBS combinational level responsible for peaks *e* and *β* could be readily deduced to be $21'^{1}33'^{1}$. The enhancement of the 28^{1} final state (peak *o*) (716 cm^{-1}) could be easily assigned to excitation of the $28'^{2}$ overtone. Note that the fundamental DBS level $28'^{1}$ corresponds to peak 12 in Fig. 2, giving rise to the resonant PE spectrum discussed in Fig. 3(j). The assignments of peaks *n*, *q*, *u*, *x* were slightly less straightforward. The combinational level $29'^{1}30'^{1}33'^{1}$ (1433 cm^{-1}) would lead to the enhancement of $30^{1}33^{1}$ (831 cm^{-1}, peak *q*), $29^{1}33^{1}$ (912 cm^{-1}, peak *u*), and $29^{1}30^{1}$ (1131 cm^{-1}, peak *β*) within our experimental accuracy. Hence, peak *β* could have contributions from both $29^{1}30^{1}$ and 21^{1} mentioned above. Similarly, the combinational level $27'^{1}44'^{1}46'^{1}$ (1425 cm^{-1}) would result in the enhancement of $27^1 46^1$ (985 cm^{-1}, peak *x*), $44^1 46^1$ (688 cm^{-1}, peak *n*), and $27^1 44^1$ (1177 cm^{-1}). The $27^1 44^1$ final state was not observed in Fig. 5(a) because it is close to the high binding energy cutoff, where the signal-to-noise ratio was poor.

Similarly, we deduced the three overlapping DBS vibrational levels (1534 cm^{-1}, Table II) that produced the complicated resonant PE spectrum in Fig. 5(b). The DBS level $32'^3 46'^1$ (1532 cm^{-1}) would autodetach to $32^2 46^1$ (1096 cm^{-1}, peak *z*) and 32^3 (1286 cm^{-1}, peak H). Note that peak H was barely observable in the non-resonant PE spectrum in Fig. 1(d). The combinational level $27'^1 29'^1 47'^1$ (1521 cm^{-1}) would autodetach to $27^1 47^1$ (928 cm^{-1}, peak *v*) and $29^1 47^1$ (787 cm^{-1}, *p*), whereas the $27^1 29^1$ level is not accessible. The combinational level $27'^1 32'^1 45'^1$ (1539 cm^{-1}) would autodetach to $32^1 45^1$ (798 cm^{-1}, peak E), $27^1 45^1$ (1115 cm^{-1}, peak *α*), and $27^1 32^1$. The latter would produce a peak around 1168 cm^{-1} above the 0–0 transition just beyond peak *α* in Fig. 5(b) but was not observed. Hence, despite the complexity of these resonant PE spectra, they could be assigned satisfactorily using the computed vibrational frequencies as a guide and using the frequencies measured from different spectra as cross checks.

D. More resonant PE spectra

Figure S2 presents 14 more resonant PE spectra and their assignments. Most of these spectra are relatively straightforward to assign. The obtained binding energies of the final states are given in Table I for all the final neutral states observed from both the resonant and non-resonant PE spectra, in comparison with the calculated frequencies and the few transitions observed by KG in the previous non-resonant PE spectra.[16] Our data are in good agreement

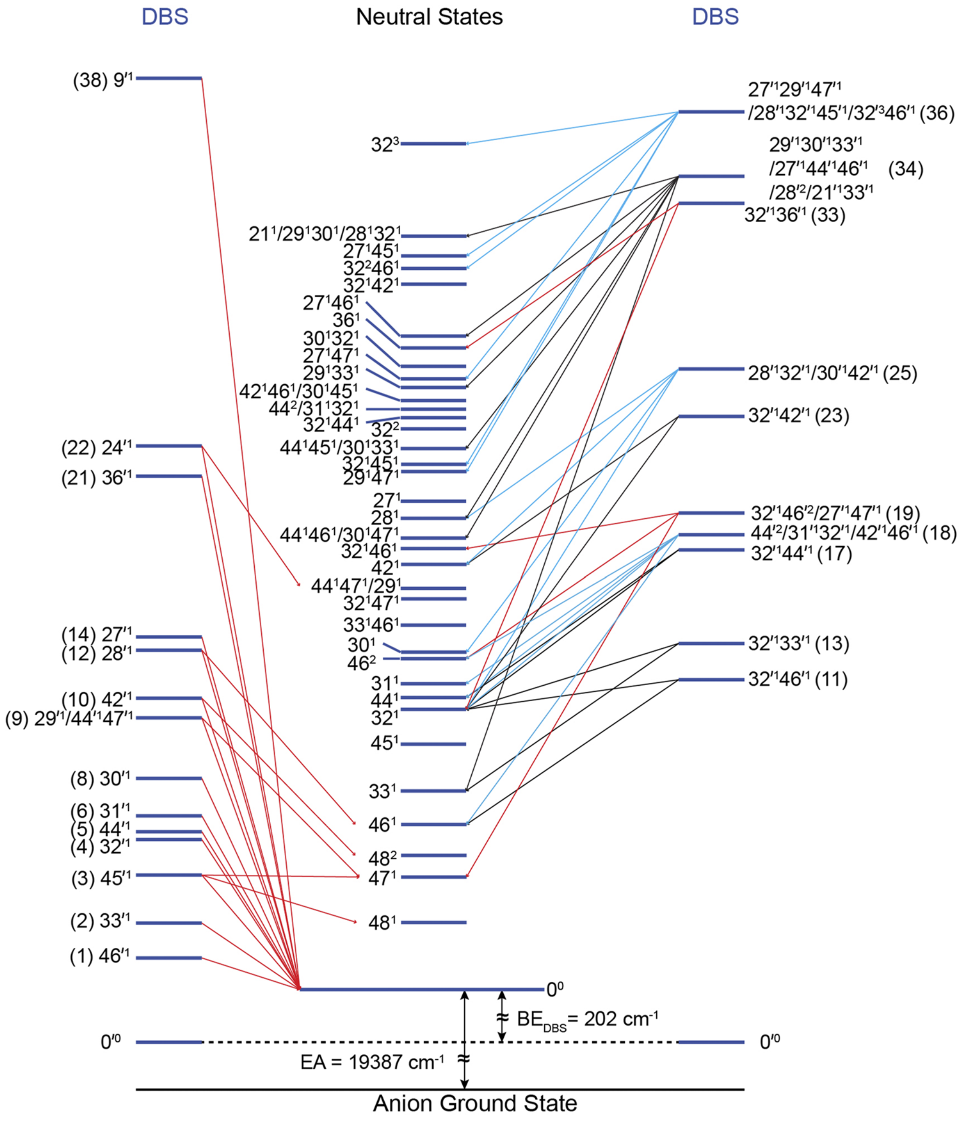

FIG. 6. Schematic energy level diagram for the vibrational autodetachment from the DBS vibrational levels of 2-naphthoxide presented in Figs. 3–5. The fundamental levels of the DBS are given in the left column, and the combinational levels are given in the right column. The peak number from Fig. 2 is given in the parentheses. The arrows indicate the autodetachment final states. The energies and assignments of the DBS levels and the final neutral levels are given in Table II and Table I, respectively.

with those reported by KG within the experimental uncertainties. However, there were two peaks in their spectra that could not be assigned definitively. One was 721 cm^{-1} above the 0-0 transition, and it was assigned to either 28^1 or $32^1 33^1$. This peak should be due to 28^1 because we did not observe $32^1 33^1$ (Table I). Interestingly, we resolved $28'^1$ (peak 12) and $32'^1 33'^1$ (peak 13) in our photodetachment spectrum (Fig. 2) and they are separated by 10 cm^{-1} (Table II). The resulting resonant PE spectra from these two DBS levels are shown in Figs. 3(j) and 4(b). The second peak that KG could not assign unambiguously was 943 cm^{-1} above the 0-0 transition, and it was assigned to either 25^1 or $30^1 32^1$. This peak corresponds to our peak G at 947 cm^{-1} above the 0–0 transition. This peak was due to the $30^1 32^1$ final state unambiguously from the current study. We observed a resonance in the photodetachment spectrum (peak 20), which corresponds to $30'^1 32'^1$, and there was no overlapping level from $25'^1$, as confirmed by the resonant PE spectrum given in Fig. S2d. Thus, the previous non-resonant PE study by KG yielded vibrational frequencies for seven vibrational modes of 2-naphthoxy: ν_{27}, ν_{28}, ν_{30}, ν_{32}, ν_{33}, ν_{45}, and ν_{46}. The ν_{45} and ν_{46} modes are out-of-plane bending modes, which were observed most likely due to vibronic couplings.[16]

E. Energy level diagrams and the rich vibrational information obtained for 2-naphthoxy

An energy level diagram is presented in Fig. 6, summarizing the autodetachment transitions from the 24 DBS levels presented in Figs. 3–5. A similar energy level diagram is given in Fig. S3, depicting the autodetachment from the 14 DBS levels shown in Fig. S2. The assignments of the 38 DBS resonances observed in the photodetachment spectra are given in Table II, in comparison with the calculated frequencies. Some of the resonant peaks are assigned to multiple vibrational levels due to accidental near-degeneracy. Since the dipole-bound electron is in a highly diffuse orbital with little effect on the neutral core, the transitions to the DBS are expected to obey the Franck–Condon principle similar to PES. Figure S1 compares the PE spectra and the photodetachment spectrum by aligning the respective 0–0 transitions. Certain similarities between the two spectra were observed indeed. However, the photodetachment spectrum was much richer in spectral features. Many transitions with low Franck–Condon factors were amplified in the photodetachment spectrum due to the resonant nature of the transitions. In particular, at high excitation energies where the PE spectrum exhibited weakening intensities, the photodetachment spectrum was still quite strong. In addition to the resonant nature of the transitions, strong vibronic couplings probably also play a role, in particular, for Franck–Condon-forbidden transitions involving bending modes. Transitions to 14 fundamental vibrational levels of the DBS were observed; the corresponding resonant PE spectra are presented in Fig. 3.

The 38 resonant PE spectra led to the observation of 36 final vibrational peaks of the 2-naphthoxy radicals, compared to only nine observed in the non-resonant PE spectra (Fig. 1). Six of these peaks contain overlapping vibrational levels, as shown in Table I, giving rise to a total of 42 final vibrational states. Combining the vibrational information from both the photodetachment spectrum and the resonant PE spectra, we obtained a total of 17 vibrational frequencies for the 2-naphthoxy radical, as summarized in Table III. Most vibrational frequencies were observed both in the photodetachment spectrum and the resonant PE spectra. The sources for each vibrational frequency are also given in Table III, where the calculated frequencies are given for comparison. The displacement vectors for these 17 normal modes are shown in Fig. S4. It is interesting to see that seven bending modes were observed, including the two lowest frequency bending modes, ν_{48} and ν_{47} with measured frequencies of 102 cm^{-1} and 171 cm^{-1}, respectively. This rich vibrational information for the 2-naphthoxy radical will be valuable to calibrate theoretical methods aimed at understanding the vibrational properties of large PAHs.

TABLE III. The observed vibrational modes and their frequencies measured in this work for the 2-naphthoxy radical.

Vibrational mode	Theo. (cm^{-1})[a]	Current work (cm^{-1})	Observed peaks[b]	Reference 16 (cm^{-1})
ν_{48} (A$''$)	103	102	a	
ν_{47} (A$''$)	171	171	b	
ν_{46} (A$''$)	254	251/248	d/1	248
ν_{45} (A$''$)	378	373/374	A/3	368
ν_{44} (A$''$)	449	444/440	f/5	
ν_{42} (A$''$)	647	646/643	l/10	
ν_{36} (A$''$)	954	975/975	w/21	
ν_{33} (A$'$)	296	302/301	e/2	303
ν_{32} (A$'$)	422	426/428	B/4	422
ν_{31} (A$'$)	462	465/464	g/6	
ν_{30} (A$'$)	517	513/521	C/8	512
ν_{29} (A$'$)	611	610/613	k/9	
ν_{28} (A$'$)	712	716/716	o/12	721
ν_{27} (A$'$)	748	742/737	D/14	743
ν_{24} (A$'$)	1018	1026	22	
ν_{21} (A$'$)	1142	1145	β	
ν_{9} (A$'$)	1580	1585	38	

[a] The theoretical frequencies come from Table S1.
[b] Peak labels from Tables I and II.

PAHs are the most abundant species in the ISM based on the observed infrared emission spectra.[12] However, no specific PAH molecules have been identified from the astronomically observed IR emission spectra because the C–H and C–C vibrations from different PAHs tend to be similar and cluster together. The low-frequency bending vibrations involving the whole PAH frameworks are expected to be the fingerprints for individual PAHs,[12] but they are very difficult to measure experimentally and compute theoretically. The current study demonstrates that photodetachment spectroscopy and resonant photoelectron spectroscopy may provide an alternative technique to obtain fingerprint vibrational information for PAHs.

V. CONCLUSIONS

In conclusion, we report an investigation of the 2-naphthoxide anion and 2-naphthoxy radical using both photodetachment spectroscopy and resonant photoelectron spectroscopy. A dipole-bound state was observed 202 cm^{-1} below the detachment threshold of the 2-naphthoxide anion. The electron affinity of the 2-naphthoxy radical was measured more accurately as 19 387(4) cm^{-1} or 2.4037(5) eV. Thirty-eight above-threshold resonances were observed in the photodetachment spectrum, which led to 38 resonantly enhanced photoelectron spectra via vibrational autodetachment. A total of 17 fundamental vibrational frequencies are measured for the 2-naphthoxy radical by combining the photodetachment and resonant photoelectron spectroscopy. Remarkably, seven bending vibrations are observed, including the two lowest frequency modes (ν_{48} and ν_{47}) with measured frequencies of 102 cm^{-1} and 171 cm^{-1}, respectively. The rich vibrational information would be valuable to calibrate theoretical methods aimed at understanding the vibrational spectra of PAHs. This study demonstrates again that the combination of photodetachment spectroscopy and resonant photoelectron spectroscopy is a powerful technique to obtain vibrational information for dipolar neutral radical species via vibrational autodetachment from the dipole-bound state.

SUPPLEMENTARY MATERIAL

See the supplementary material for the full set of calculated vibrational frequencies for the 2-naphthoxy radical, comparison of the non-resonant photoelectron spectrum with the photodetachment spectrum and a Franck–Condon simulation, additional resonant photoelectron spectra that are not discussed in the main text and the related energy level diagram, and the 17 observed normal modes of vibration.

ACKNOWLEDGMENTS

This work was supported by the U.S. Department of Energy, Office of Basic Energy Sciences, Chemical Science, Geosciences, and Bioscience Division under Grant No. DE-SC0018679.

DATA AVAILABILITY

The data that support the findings of this study are available from the corresponding author upon reasonable request.

REFERENCES

[1] M. Panizza, P. A. Michaud, G. Cerisola, and C. Comninellis, J. Electroanal. Chem. **507**, 206–214 (2001).

[2] M. Smrcina, S. Vyskocil, B. Maca, M. Polasek, T. A. Claxton, A. P. Abbott, and P. Kocovsky, J. Org. Chem. **59**, 2156–2163 (1994).

[3] T. Pielhop, J. Amgarten, M. H. Studer, and P. R. von Rohr, Biotech. Biofuels **10**, 130 (2017).

[4] H. Zollinger, *Color Chemistry* (Wiley VCH, Weinheim, 2003), p. 637.

[5] N. Agmon, J. Phys. Chem. A **109**, 13–35 (2005).

[6] J. Lee, R. D. Griffin, and G. W. Robinson, J. Chem. Phys. **82**, 4920–4925 (1985).

[7] M. Lawrence, C. J. Marzzacco, C. Morton, C. Schwab, and A. M. Halpern, J. Phys. Chem. **95**, 10294–10299 (1991).

[8] H. K. Chagger, J. M. Jones, M. Pourkashanian, A. Williams, A. Owen, and G. Fynes, Fuel **78**, 1527–1538 (1999).

[9] A. W. H. Chan, K. E. Kautzman, P. S. Chhabra, J. D. Surratt, M. N. Chan, J. D. Crounse, A. Kürten, P. O. Wennberg, R. C. Flagan, and J. H. Seinfeld, Atmos. Chem. Phys. **9**, 3049–3060 (2009).

[10] M. P. Bernstein, J. E. Elsila, J. P. Dworkin, S. A. Sandford, L. J. Allamandola, and R. N. Zare, Astrophys. J. **576**, 1115–1120 (2002).

[11] M. P. Bernstein, J. P. Dworkin, S. A. Sandford, and L. J. Allamandola, Adv. Space Res. **30**, 1501–1508 (2002).

[12] A. G. G. M. Tielens, Annu. Rev. Astron. Astrophys. **46**, 289–337 (2008).

[13] P. K. Das, M. V. Encinas, S. Steenken, and J. C. Scaiano, J. Am. Chem. Soc. **103**, 4162–4166 (1981).

[14] M. Sekine, H. Sekiya, and M. Nakata, J. Phys. Chem. A **116**, 8980–8988 (2012).

[15] W. T. Dixon, W. E. J. Foster, and D. Murphy, J. Chem. Soc. Perkin Trans. **2**, 2124–2127 (1973).

[16] S. J. Kregel and E. Garand, J. Chem. Phys. **149**, 074309 (2018).

[17] J. N. Bull, J. T. Buntine, M. S. Scholz, E. Carrascosa, L. Giacomozzi, M. H. Stockett, and E. J. Bieske, Faraday Discuss. **217**, 34–46 (2019).

[18] C.-H. Qian, G.-Z. Zhu, and L.-S. Wang, J. Phys. Chem. Lett. **10**, 6472–6477 (2019).

[19] R. L. Jackson, A. H. Zimmerman, and J. I. Brauman, J. Chem. Phys. **71**, 2088–2094 (1979).

[20] K. R. Lykke, R. D. Mead, and W. C. Lineberger, Phys. Rev. Lett. **52**, 2221–2224 (1984).

[21] C. Desfrançois, H. Abdoul-Carime, and J.-P. Schermann, Int. J. Mod. Phys. B **10**, 1339–1395 (1996).

[22] N. I. Hammer, K. Diri, K. D. Jordan, C. Desfrançois, and R. N. Compton, J. Chem. Phys. **119**, 3650–3660 (2003).

[23] N. I. Hammer, R. J. Hinde, R. N. Compton, K. Diri, K. D. Jordan, D. Radisic, S. T. Stokes, and K. H. Bowen, J. Chem. Phys. **120**, 685–690 (2004).

[24] K. D. Jordan and F. Wang, Annu. Rev. Phys. Chem. **54**, 367–396 (2003).

[25] L.-S. Wang, J. Chem. Phys. **143**, 040901 (2015).

[26] H.-T. Liu, C.-G. Ning, D.-L. Huang, P. D. Dau, and L.-S. Wang, Angew. Chem., Int. Ed. **52**, 8976–8979 (2013).

[27] D.-L. Huang, G.-Z. Zhu, and L.-S. Wang, J. Chem. Phys. **142**, 091103 (2015).

[28] D.-L. Huang, H.-T. Liu, C.-G. Ning, and L.-S. Wang, J. Chem. Phys. **142**, 124309 (2015).

[29] D.-L. Huang, C.-G. Ning, H.-T. Liu, and L.-S. Wang, J. Phys. Chem. Lett. **6**, 2153–2157 (2015).

[30] D.-L. Huang, G.-Z. Zhu, Y. Liu, and L.-S. Wang, J. Mol. Spectrosc. **332**, 86–93 (2017).

[31] D.-L. Huang, H.-T. Liu, C.-G. Ning, P. D. Dau, and L.-S. Wang, Chem. Phys. **482**, 374–383 (2017).

[32] G.-Z. Zhu, D.-L. Huang, and L.-S. Wang, J. Chem. Phys. **147**, 013910 (2017).

[33] G.-Z. Zhu, C.-H. Qian, and L.-S. Wang, J. Chem. Phys. **149**, 164301 (2018).

[34] G. Z. Zhu, C. H. Qian, and L. S. Wang, Angew. Chem., Int. Ed. **58**, 7856–7860 (2019).

[35] G.-Z. Zhu, L. F. Cheung, Y. Liu, C.-H. Qian, and L.-S. Wang, J. Phys. Chem. Lett. **10**, 4339–4344 (2019).

[36] J. Czekner, L. F. Cheung, G. S. Kocheril, and L.-S. Wang, Chem. Sci. **10**, 1386–1391 (2019).

[37] H.-T. Liu, C.-G. Ning, D.-L. Huang, and L.-S. Wang, Angew. Chem., Int. Ed. **53**, 2464–2468 (2014).

[38] D.-L. Huang, H.-T. Liu, C.-G. Ning, G.-Z. Zhu, and L.-S. Wang, Chem. Sci. **6**, 3129–3138 (2015).

[39] G.-Z. Zhu and L.-S. Wang, Chem. Sci. **10**, 9409–9423 (2019).

[40] L.-S. Wang, C.-F. Ding, X.-B. Wang, and S. E. Barlow, Rev. Sci. Instrum. **70**, 1957–1966 (1999).

[41] X.-B. Wang and L.-S. Wang, Rev. Sci. Instrum. **79**, 073108 (2008).

[42] I. León, Z. Yang, H.-T. Liu, and L.-S. Wang, Rev. Sci. Instrum. **85**, 083106 (2014).

[43] G. A. Garcia, L. Nahon, and I. Powis, Rev. Sci. Instrum. **75**, 4989–4996 (2004).

[44] V. Dribinski, A. Ossadtchi, V. A. Mandelshtam, and H. Reisler, Rev. Sci. Instrum. **73**, 2634–2642 (2002).

[45] M. J. Frisch, G. W. Trucks, H. B. Schlegel, G. E. Scuseria, M. A. Robb, J. R. Cheeseman, G. Scalmani, V. Barone, B. Mennucci, G. A. Petersson, H. Nakatsuji, M. Caricato, X. Li, H. P. Hratchian, A. F. Izmaylov, J. Bloino, G. Zheng,

J. L. Sonnenberg, M. Hada, M. Ehara, K. Toyota, R. Fukuda, J. Hasegawa, M. Ishida, T. Nakajima, Y. Honda, O. Kitao, H. Nakai, T. Vreven, J. A. Montgomery, Jr., J. E. Peralta, F. Ogliaro, M. Bearpark, J. J. Heyd, E. Brothers, K. N. Kudin, V. N. Staroverov, R. Kobayashi, J. Normand, K. Raghavachari, A. Rendell, J. C. Burant, S. S. Iyengar, J. Tomasi, M. Cossi, N. Rega, J. M. Millam, M. Klene, J. E. Knox, Jr., B. Cross, V. Bakken, C. Adamo, J. Jaramillo, R. Gomperts, R. E. Stratmann, O. Yazyev, A. J. Austin, R. Cammi, C. Pomelli, J. W. Ochterski, R. L. Martin, K. Morokuma, V. G. Zakrzewski, G. A. Voth, P. Salvador, J. J. Dannenberg, S. Dapprich, A. D. Daniels, Ö. Farkas, J. B. Foresman, J. V. Ortiz, J. Cioslowski, and D. J. Fox, Gaussian 09, Revision C.01, Gaussian, Inc., Wallingford CT, 2010.

[46] E. P. Wigner, Phys. Rev. **73**, 1002–1009 (1948).

[47] R. S. Berry, J. Chem. Phys. **45**, 1228–1245 (1966).

[48] J. Simons, J. Am. Chem. Soc. **103**, 3971–3976 (1981).